Front. Optoelectron. 2021, 14(4): 473–481
https://doi.org/10.1007/s12200-021-1236-y

RESEARCH ARTICLE

Oxide perovskite Ba_2AgIO_6 wafers for X-ray detection

Longbo YANG, Jincong PANG, Zhifang TAN, Qi XIAO, Tong JIN, Jiajun LUO (✉), Guangda NIU, Jiang TANG

Wuhan National Laboratory for Optoelectronics (WNLO), School of Optical and Electronic Information, Huazhong University of Science and Technology, Wuhan 430074, China

Abstract X-ray detection is of great significance in biomedical, nondestructive, and scientific research. Lead halide perovskites have recently emerged as one of the most promising materials for direct X-ray detection. However, the lead toxicity remains a worrisome concern for further commercial application. Great efforts have been made to search for lead-free perovskites with similar optoelectronic properties. Here, we present a lead-free oxide double perovskite material Ba_2AgIO_6 for X-ray detection. The lead-free, all-inorganic nature, as well as the high density of Ba_2AgIO_6, promises excellent prospects in X-ray applications. By employing the hydrothermal method, we successfully synthesized highly crystalline Ba_2AgIO_6 powder with pure phase. Furthermore, we prepared Ba_2AgIO_6 wafers through isostatic pressure and built X-ray detectors with Au/Ba_2AgIO_6 wafer/Au photoconductive structure. The as-prepared X-ray detectors showed a sensitivity of 18.9 μC/(Gy_{air}·cm^2) at 5 V/mm, similar to commercial α-Se detectors showcasing their advantages for X-ray detection.

Keywords oxide double perovskite, lead-free, X-ray detection

1 Introduction

X-ray detection has attracted significant attention for various applications, including medical diagnostics, computed tomography, nondestructive inspection, and scientific research [1,2]. Generally, there are two methods to realize X-ray detection: indirect detection and direct detection. Compared with the indirect strategy, which converts X-ray to photons by scintillators [3], the direct X-ray detection, that converts X-ray radiation directly into the electrical response, is considered to have great potential due to its simple system and high spatial resolution [4,5]. Among X-ray detection materials used for direct detection, metal halide perovskites have recently shown huge prospects due to their high average atomic number, considerable mobility–lifetime product ($\mu\tau$), high defect tolerance, and simple preparation process [6–8].

However, lead in metal halide perovskites is a significant obstacle to its application in X-ray detection. For example, to absorb 99% of the X-rays at 50 keV, $MAPbBr_3$, a promising X-ray detect material, requires a 2.3-mm-thick flat-panel containing a total Pb of 3836 g/m^2, much significantly higher than the EU RoHS regulation limit of 1000 ppm Pb [9]. Therefore, replacing the Pb with non-toxic metal in practical application is necessary [10–12]. Among prospective candidates, double perovskites have been proved as a highly suitablealternative. $Cs_2AgBiBr_6$ has been reported to achieve high sensitivity with 105 μC/(Gy_{air}·cm^2) and a low detection limit with 36 nGy_{air}/s [13].

Nevertheless, the density of metal halide perovskites is relatively small for an ideal X-ray detector. For example, the density of $MAPbBr_3$ is 3.582 g/cm^3, and the density of $Cs_2AgBiBr_6$ is 4.954 g/cm^3, which is still lower than the density of CdTe (6.2 g/cm^3), a material usually used in direct detection. Therefore, perovskite materials with combined characteristics of non-lead and high density are highly desired for X-ray detection.

Ba_2AgIO_6 has newly emerged as a lead-free oxide double perovskite with a cubic structure with the centers of metal-oxygen octahedron occupied by $Ag^+$and I^{7+} [14], which was first reported by Volonakis et al. Ba_2AgIO_6 possesses great advantages in X-ray detection: 1) Large absorption coefficient. It is much denser than metal halide perovskites and slightly denser than CdTe (The density of Ba_2AgIO_6 is 6.411 g/cm^3, the density of $Cs_2AgBiBr_6$ is 4.954 g/cm^3, and the density of CdTe is 6.2 g/cm^3). 2) Appropriate bandgap structure. It has a bandgap of 1.9 eV, making it ideal for X-ray detection [14] (Larger bandgap would lead to a decrease in conversion efficiency, and a smaller bandgap would lead to an increase in hot carriers). 3) Low ion migration oxides have a more stable

Received April 23, 2021; accepted June 3, 2021

E-mail: luojiajun@mail.hust.edu.cn

crystal structure, which can effectively inhibit ion migration [15,16]. Thereby, we believe that Ba_2AgIO_6 and a series of oxide double perovskites represented by Ba_2AgIO_6 are very promising in applying X-ray detection.

Despite holding great promises, the optoelectronic applications of Ba_2AgIO_6 have not been widely researched. Thus, in this study, we focus on the sample quality improvement, and the application of oxide double perovskite Ba_2AgIO_6 for a sensitive X-ray detector. We synthesized high crystallinity Ba_2AgIO_6 powder by hydrothermal instead of a low-temperature solution process, prepared a Ba_2AgIO_6 wafer by isostatic pressure to satisfy the upscaling ability, and further built the direct X-ray detector with Au/Ba_2AgIO_6/Au structure. Thanks to the above suitable process and Ba_2AgIO_6 itself excellent nature, our detector's X-ray sensitivity is 18.9 μC/($Gy_{air}\cdot cm^2$) at 5 V bias (about 5 V/mm), which is comparable to commercial α-Se X-ray detectors (20 μC/($Gy_{air}\cdot cm^2$)) [17].

2 Experimental section

Materials and chemicals: Barium hydroxide ($Ba(OH)_2\cdot 8H_2O$, 98%), silver oxide (Ag_2O, 99.99%), and periodic acid (HIO_4, 99.9%) were purchased from Alfa Aesar. Nitric acid (HNO_3, 65 wt% – 68 wt% in water) and acetonitrile (CH_3CN, 99.8%) were procured from Sinopharm Chemical Reagent Co., Ltd., China. All materials and chemicals were used without further purification unless otherwise noted.

Synthesis of Ba_2AgIO_6 powder: Ba_2AgIO_6 powder was grown from mixed solvents in equal proportions of water and acetonitrile by hydrothermal method. 630.92 mg (2 mmol) $Ba(OH)_2\cdot 8H_2O$, 298.769 mg (1 mmol) $AgIO_4$, and 20 mL acetonitrile and 20 mL H_2O were first loaded into a PTFE container successively. The PTFE container was then heated to 180°C in a hydrothermal kettle for 10 h. After another 20 h of slow cooling, the Ba_2AgIO_6 powder was successfully synthesized. The obtained powder was rinsed with water three times to remove surface impurities and organic solvents and dried in an oven for subsequent preparation of the wafer.

Structural characterization: X-ray diffraction (XRD) experiments were performed by X'Pert3 Powder (PANalytical B.V using a Cu Kα rotating anode). X-ray fluorescence experiments were conducted by EAGLE III (EDAX Inc. using A1 Kα excitation)

Optical characterization: The UV-Vis absorption spectrum was measured by a UV-visible spectrophotometer (SolidSpec-3700, Shimadzu). Fluorescence spectra were examined by a transient/steady-state fluorescence spectrometer (FLS 920) with a 325 nm laser.

X-ray detector fabrication and characterization: The as-prepared powder was modeled into a pie shape by a compressor under 4 MPa pressure. Subsequently, it was loaded in an elastic mold made of latex and put into an isostatic pressing machine with an oil bath under 200 MPa for 5–10 min. After the oil on the mold is dried, the wafer was transferred into a thermal evaporation machine. 50 nm-thick gold with an area of 2 mm×5 mm was evaporated on both sides at a rate of 1 Å/s. For X-ray detector characterization, we used a gold anode X-ray tube (Newton Scientific M237) with a maximum output of 10 W as our X-ray source and used the Keithley 6571B semiconductor characterization system as a voltage source and a device for measuring current and voltage. We controlled the X-ray dose by changing the current of the X-ray tube from 140 to 10 μA with a constant working voltage of 50 keV. All the X-ray characterization was conducted in a lead box to minimize interference from ambient noise and light.

X-ray dose calibration: We calibrated the X-ray dose rate using the MagicMax ion chamber dosimeter from IBA Dosimetry. First, the X-ray tube is fixed in a specific position with a working distance of 10 cm. Then the dose rate was measured at 50 kV working voltage. We adjust the dose rate during this process by changing the working current of the X-ray tube from 140 to 10 μA. Finally, remove the dosimeter, and place the sample to be tested in this position. If you need to simulate other working scenarios, you can adjust the voltage as appropriate or add the aluminum plate for attenuation. The radiation dose rate of the X-ray tube is not the same as the actual absorbed dose rate of the sample, which is affected by many factors, such as distance, position (heel effect), air attenuation, sample area, and other factors. Therefore, we use Gy_{air}/s in the article, which is the absorbed dose rate obtained from the dosimeter, to refer to the actual absorbed dose rate of the sample.

3 Results and discussion

We focus on Ba_2AgIO_6 for potential X-ray detection. The absorption is such an important property in X-ray detection that we first calculate the absorption coefficients of Ba_2AgIO_6, $MAPbBr_3$, $Cs_2AgBiBr_6$, Si, and CdTe for photons in the range of 0.01 to 100 MeV using the photon cross-section database [18]. As shown in Fig. 1(a), the absorption coefficient of Ba_2AgIO_6 across the energy region we calculated is much higher than that of $MAPbBr_3$, and comparable to the value for CdTe. The large density of Ba_2AgIO_6 enables such high absorption coefficient. To determine the X-ray detector thickness, we further calculate the attenuation spectra of these materials for hard X-rays at 50 keV. For 50 keV X-ray photons, a 0.7 mm thickness of Ba_2AgIO_6 is sufficient to absorb 99% X-rays, while 2.3 mm is required for $MAPbBr_3$ (Fig. 1(b)) [19], indicating a higher X-ray attenuation coefficient of Ba_2AgIO_6.

In addition to the absorption coefficient, the electronic bandgap is also important for X-ray detection [20]. The

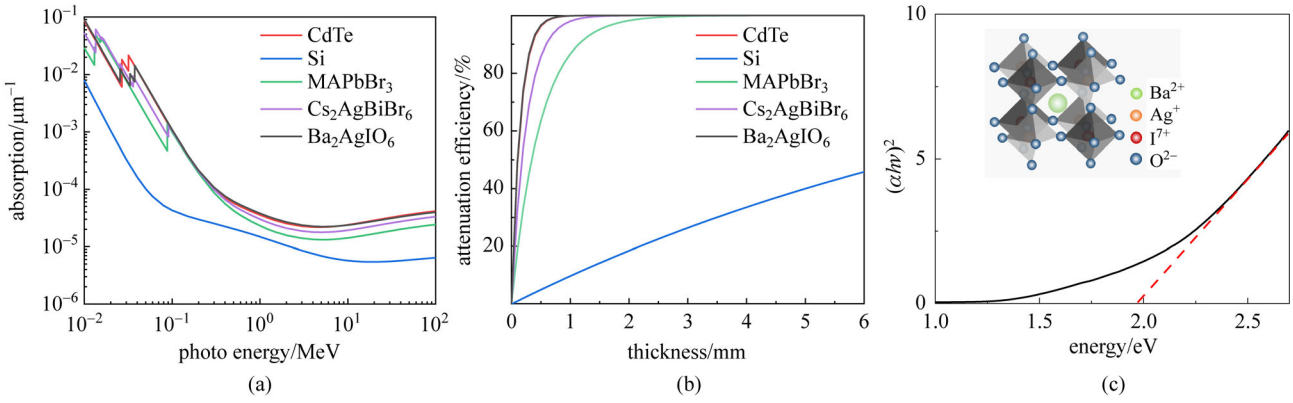

Fig. 1 (a) Absorption coefficients of Ba_2AgIO_6, Si, $MAPbBr_3$, $Cs_2AgBiBr_6$, and CdTe from soft X-rays to gamma rays. (b) Attenuation efficiencies of Ba_2AgIO_6, Si, $MAPbBr_3$, $Cs_2AgBiBr_6$, and CdTe at different thickness. (c) Crystal structure of Ba_2AgIO_6 and the fitted bandgap width (1.9 eV)

moderate bandgap provides a higher current response while avoiding the noise generated by hot carriers (The smaller the energy band, the higher the current response, and the higher the hot carrier concentration). The bandgap of Ba_2AgIO_6 fits to be 1.9 eV (Fig. 1(c)), which is smaller than that of $CsPbBr_3$ (2.3 eV) and larger than that of Si (1.1 eV).

Volonakis et al. prepared Ba_2AgIO_6 by mixing acetonitrile solution of $AgIO_4$ with the aqueous solution of $Ba(OH)_2$, and Ba_2AgIO_6 was directly precipitated from the solution [14]. However, the as-prepared Ba_2AgIO_6 powder shows inferior quality with broad photoluminescence, which is not ideal for a high-performance detector. The low-temperature solution process (LTSP) possesses the disadvantage of insufficient solvent mixing and fast precipitating.

Thus, we improved his method, using the mixed solvent hydrothermal method to prepare Ba_2AgIO_6 powder. This method adjusts the crystallization speed by controlling the temperature gradient and obtains high-quality powders [21]. In preparing Ba_2AgIO_6, it is necessary to add an appropriate amount of acetonitrile in the solvent due to the poor solubility of $AgIO_4$ in water. We adjusted the acetonitrile and water ratio to 1:1 after several tries to ensure a complete and uniform reaction.

As illustrated in Fig. 2(a), Ba_2AgIO_6 prepared by the improved hydrothermal method shows narrower XRD peak, indicating its higher crystallinity. The complete match between XRD patterns and calculated results indicates a pure phase of as-prepared Ba_2AgIO_6. Besides, we used X-ray fluorescence (XRF) measurement to verify the composition of its elements (Table S1), the content of Ba, Ag, and I match with 2:1:1. Moreover, we measured the photoluminescence spectrums of Ba_2AgIO_6 powder prepared by both methods (Fig. 2(b)). Ba_2AgIO_6 powder prepared by hydrothermal processes records narrow half peak width, and also confirms its high crystallinity.

Based on high-quality Ba_2AgIO_6 powder, we explored the preparation of the Ba_2AgIO_6 X-ray detector. It is still difficult to prepare the large-area and millimeter-thick X-ray detector. The traditional solution process leaves the pinholes in the film, which blocks the transmission of carries. In comparison, the whole process of isostatic-pressing is free of solution avoiding the drawback [7,22]. In addition, during the process preparation by solution process, the oxidizing $AgIO_4$ and alkaline $Ba(OH)_2$ reduce the selectivity of the substrate and hinder the preparation of flat-panel [23]. Thereby, we finally turned to an isostatic-pressing method for Ba_2AgIO_6 film fabrication, as shown in Fig. 2(c) [7].

We preloaded the powder mechanically at 4 MPa to ensure the size and shape of the wafer. Ball mill is needed for the raw material to ensure that the grain size is uniform and the wafer's shape is regular. Otherwise, the wafer is liable to crack during further operation due to the pressure's unevenness on it. Then, the repressed wafers were loaded into an elastic mold made of latex in an oil bath. The fabrication could be completed after applying 200 MPa pressure to the oil for 5–10 min.

We characterized the wafers' surface by scanning electron microscope (SEM) image, based on obtaining the wafer. The top-view surface SEM image shows a compact, flat, and pinhole-free morphology at 10 μm scale bar (Fig. 2(a)), which is beneficial for minimizing leakage current for direct X-ray detection. As illustrated in Figs. S2(b) and S2(c), the powder's grain size is about 20 – 50 nm, which is consistent with the grain size of the wafer we measured. The grain size barely changed after isostatic pressure, and we believe this is primarily because Ba_2AgIO_6 is an oxide semiconductor with stronger covalence and is challenging to grow during the process of isostatic pressure without annealing [24].

Finally, Ba_2AgIO_6 thick-wafers-based X-ray detectors with a photoconductive vertical structure were fabricated

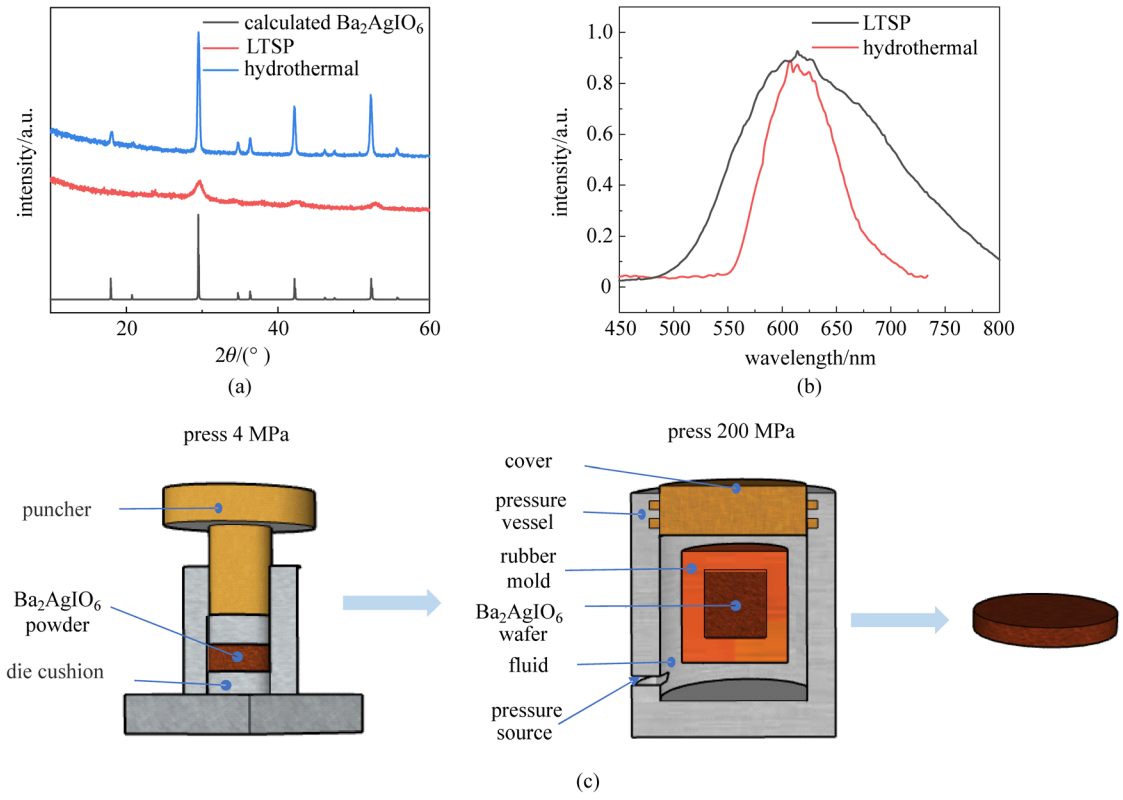

Fig. 2 (a) X-ray diffraction (XRD) data of the powders synthesized by hydrothermal method and a low-temperature solution process (LTSP). (b) Photoluminescence spectrum of the powders synthesized by different methods. (c) Schematic of preparation of Ba_2AgIO_6 wafers by cold isostatic pressing

as Fig. 3(a). A 50 nm gold electrode is evaporated on both sides of the 1 mm thick wafer with a size of 2 mm×5 mm. After a voltage was applied to both ends of the electrode, X-rays shined from one side of the gold electrode (Fig. 3(a)). All tests were performed with a 50 keV X-ray tube (Newton Scientific M237). We adjust the dose rate of X-rays by changing the amount of current. We focus on the performance of the devices prepared by the hydrothermal method and mixed precipitation method.

As expected, the detectors' performance prepared by the hydrothermal method is much higher than that prepared by a low-temperature solution process. The former one has a lower dark current (1.22 nA) and a higher photon response (3.06 nA), while the latter has a higher dark current (6.08 nA) and a lower photon response (0.88 nA) (Fig. 3(b)). Figure 3(c) shows the response pattern of the hydrothermal device with the X-ray dose rate from 5499 to 785 $\mu Gy_{air}/s$ by changing the current of the X-ray source from 140 to 20 μA at a constant DC bias of 5 V. It should be noted that the contribution of air ionization can be ignored because of the considerable difference between the response of air ionization and that of our device (Fig. S4). Here, we consider that the electrode area size is 0.1 cm^2. We can estimate the ray detection sensitivity under different bias voltages by linear fitting according to this data. The result is reported in Fig. 3(d). The X-ray detection sensitivity of the Ba_2AgIO_6 device is calculated to be about 4.05 $\mu C/(Gy_{air}\cdot cm^2)$ at 1 V bias (about 1 V/mm) and 18.9 $\mu C/(Gy_{air}\cdot cm^2)$ at 5 V bias (about 5 V/mm). We further compared the responses of wafers with different thicknesses (Table S2). According to Fig. 1(b), the 0.7 mm thickness of Ba_2AgIO_6 is sufficient to absorb 99% of X-rays. Therefore, the 0.5 mm-thick wafer cannot fully absorb X-rays, resulting in a significant loss of sensitivity. For a 2 mm-thick wafer device, photogenerated carriers cannot reach both ends of the electrode due to the poor charge transportability of our Ba_2AgIO_6 wafer, leading to the decrease of our device's sensitivity. After considering factors such as X-ray absorption and charge transfer, We obtained the optimal X-ray sensitivity of 18.9 $\mu C/(Gy_{air}\cdot cm^2)$ at 5 V of the device at 1 mm thickness. The sensitivity is very close to commercial α-Se X-ray detectors (20 $\mu C/(Gy_{air}\cdot cm^2)$) [17]. Its relatively good sensitivity and non-lead toxicity fully demonstrate its application in X-ray detection.

Further, we analyze the physical process of the Ba_2AgIO_6 X-ray detector. Because the X-ray energy is relatively low and the atomic number of Ba_2AgIO_6 is relatively high, the primary process of our device is the photoelectric process rather than the Compton scattering process. In detail, the process generates high-energy electrons that lose their energy subsequently in relaxation with producing more pairs of electron holes [24].

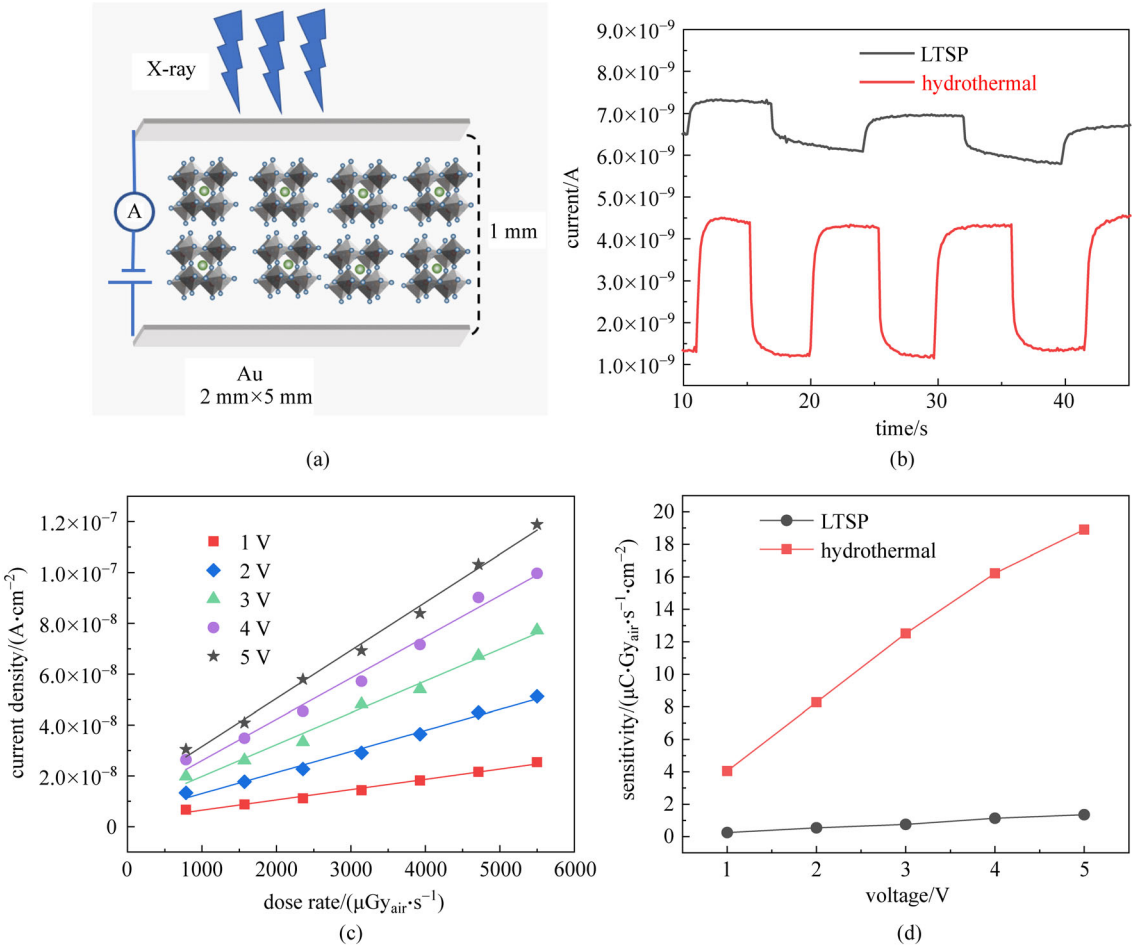

Fig. 3 (a) Device structure of Ba_2AgIO_6 X-ray detector. (b) Response for devices prepared by hydrothermal method and mixed precipitation at 785 μGy$_{air}$/s X-ray dose rate at 5 V bias. (c) Response for devices prepared by hydrothermal method from 5499 to 785 μGy$_{air}$/s X-ray dose rate and 1 to 5 V bias. (d) X-ray sensitivity of devices prepared by hydrothermal method and mixed precipitation method at different bias voltages

For our detector, we focus on its theoretical sensitivity and gain factor. According to the empirical formula $\Delta E = 1.43 + 2E_g$ [25], the energy loss for generating one electron-hole pair (ΔE) known as the ionization energy for Ba_2AgIO_6 can be evaluated to be 5.29 eV. Based on the ionization energy, we can calculate the theoretical sensitivity of the Ba_2AgIO_6 X-ray detector by

$$S_0 = \frac{\frac{\phi}{X}\overline{E}\beta}{\Delta E} e\eta,$$

where ϕ/X is the number of photons per unit of exposure, $\overline{E}$ is the mean energy of X-ray photons, β is the energy absorption efficiency of X-ray, and η is the gain factor (β and η can be considered as 100% in calculating). The theoretical sensitivity of the Ba_2AgIO_6 X-ray detector is 1279 μC/(Gy$_{air}$·cm^2).

As for the gain factor, which can also be called current collection efficiency, it can be calculated by $G = I_R/I_P$ [8,26,27]. Here, I_R is the signal current, and I_P is the theoritical current. Finally, we got the gain factor under different dose rates and electric fields (Fig. S5). As the irradiation increases, the gain factor decreases because of the filling in the shallow defect by photonic carriers [28]. That phenomenon is widely observed in photoconductive photodetectors [29].

To quantitatively characterize the stability of our detectors, we recorded the stability of the wafers. The wafers were exposed to the air for 60 days, and changes in their XRD and X-ray sensitivity were mainly observed. We tested the XRD at the beginning, the 20 days, the 40 days, and the 60 days. As Fig. 4(a) shown, the XRD of the device had some tiny burrs on the 20 days. On the 40 days, these mixed peaks increased, and on the 60 days, the mixed peaks became more apparent, indicating that the material might have decomposed at this time. We speculate that

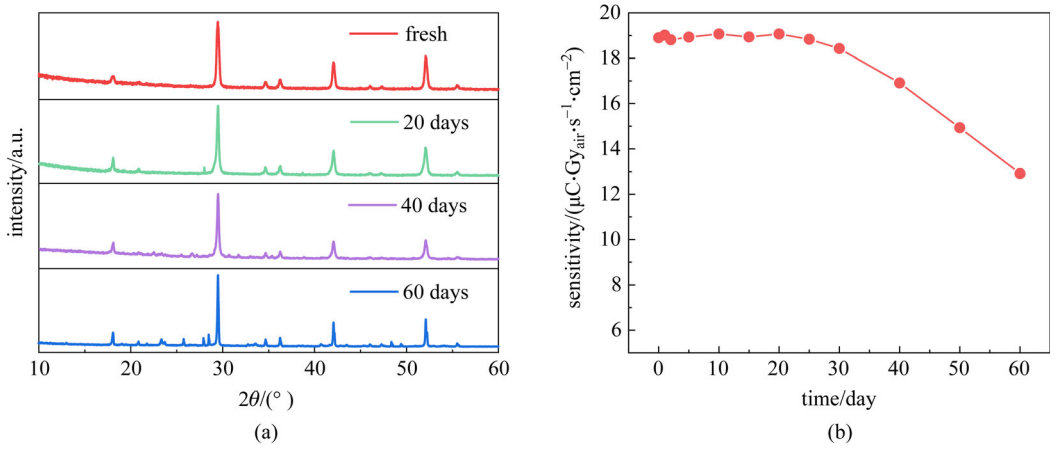

Fig. 4 (a) X-ray diffraction (XRD) data of Ba_2AgIO_6 powder exposed in air for different time. (b) X-ray sensitivity of Ba_2AgIO_6 X-ray detector exposed in air for different time

this phenomenon comes from the unstable high price state of I^{7+}.

Consistent with the XRD data, the sensitivity of the X-ray decreased with the increase of storage time. The inflection point of decreasing sensitivity appeared on the 20th day, and it finally dropped to 12.91 μC/(Gy_{air}·cm^2) on the 60th day, which was 68% of the original value (Fig. 4(b)). In general, the device's stability remains good in a short period, but due to the high-priced I^{7+}, it is not suitable to be stored in the air for a long time. Thus, an appropriate packaging process needs to be considered.

4 Conclusions

In conclusion, we report a Ba_2AgIO_6 direct X-ray detector.

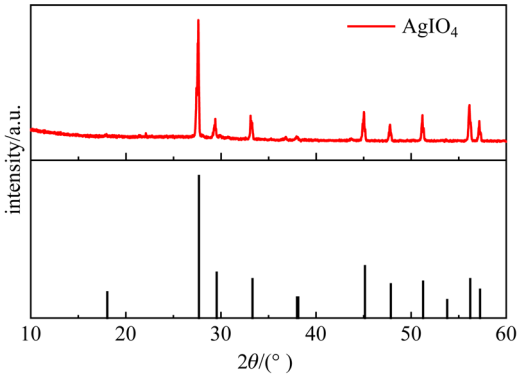

Fig. S1 X-ray diffraction (XRD) data of $AgIO_4$

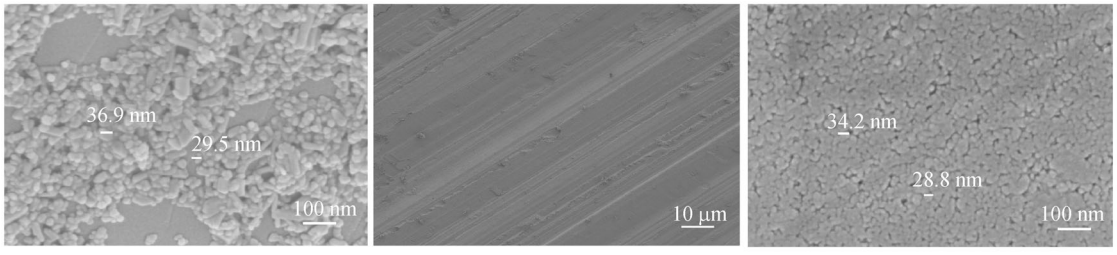

Fig. S2 (a) Scanning electron microscope (SEM) image of Ba_2AgIO_6 powder. (b) SEM image of Ba_2AgIO_6 wafer at 10 μm scalebar. (c) SEM image of Ba_2AgIO_6 wafer at 100 nm scalebar

Table S1 X-ray fluorescence (XRF) data of Ba_2AgIO_6

	Ag/%	I/%	Ba/%
sample 1	27.06	21.59	51.35
sample 2	27.12	24.57	48.31
sample 3	25.91	22.86	51.42
sample 4	23.32	24.18	52.49

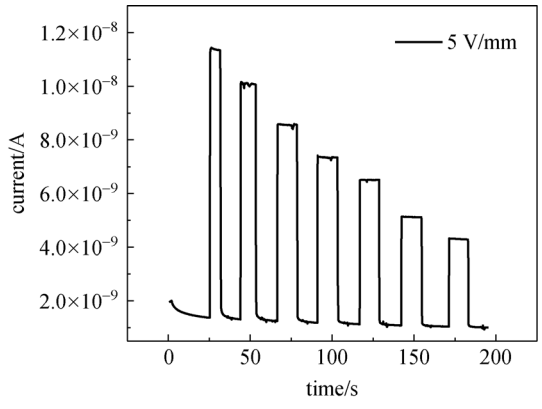

Fig. S3 Response for devices prepared by hydrothermal method from 5499 to 785 $\mu Gy_{air}/s$ X-ray dose rate at 5 V bias

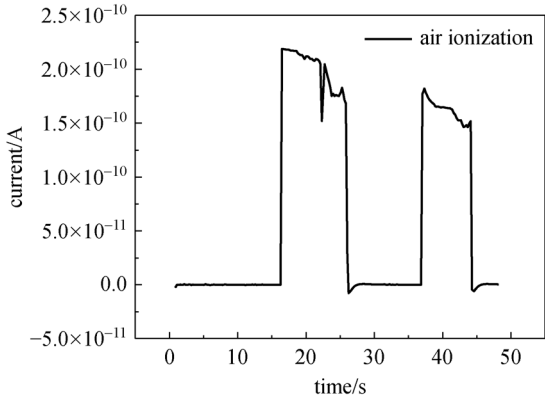

Fig. S4 Air ionization response with the same probes' position at 5499 and 4713.5 $\mu Gy_{air}/s$ X-ray dose rate at 5 V bias

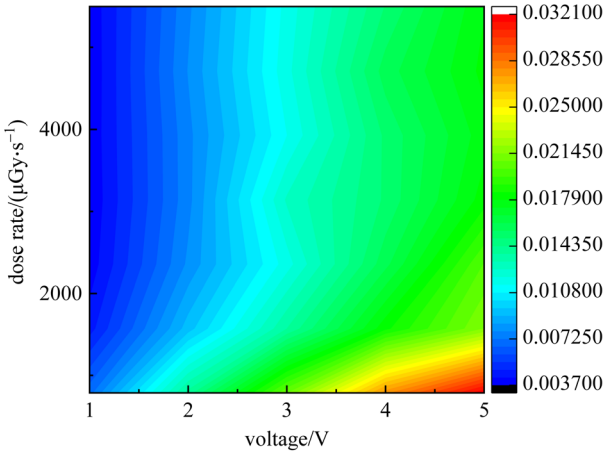

Fig. S5 Photoconductive gain factor under different dose rates and electric fields

We have improved the mixed precipitation process, synthesized high-quality Ba_2AgIO_6 powder using the mixed solvent hydrothermal. Compared with the powder synthesized by a low-temperature process, our powder possesses a higher purity and crystallinity. Then, a 1 cm diameter wafer was prepared by cold-isostatic-pressing. In this way, we can fabricate a large area X-ray plate detector to avoid the solution process's pinholes. Finally, a simple X-ray detector was prepared by steaming electrodes on both ends of the wafer. Its response at a bias voltage of 5 V is as high as 18.9 $\mu C/(Gy_{air} \cdot cm^2)$, comparable to the commercial α-Se X-ray detectors' performance. This work shows its promise in the field of X-ray detection.

Acknowledgements This work was financially supported by the National Postdoctoral Program for Innovative Talent (No. BX20200142), the National Natural Science Foundation of China (Grant Nos. 61725401, 5171101030, and 51761145048), the National Key R&D Program of China (Nos. 2016YFB0700702, 2016YFA0204000, and 2016YFB0201204), the HUST Key Innovation Team for Interdisciplinary Promotion (No. 2016JCTD111), and China Postdoctoral Science Foundation (Nos. 2020M62004075 and 2020M62005089). The authors from HUST thank the Analytical and Testing Center of HUST and the facility support of the Center for Nanoscale Characterization and Devices, WNLO. We also thank Prof. Guangzu Zhang for providing the isostatic pressing machine.

Supporting Information

Influenced by the shallow defect, the photogenerated carriers will travel between the electrodes many times, leading to the photocurrent's gain. The gain factor (G) can be defined as $G = I_R/I_P$, where I_R is the signal current we measured, and I_P is the theoretical current. The theoretical current can be calculated as $I_P = \varnothing\beta e$, where $\varnothing$ is the photon absorption rate, and β is the maximum number of photogenerated carries per photon. The photon absorption rate $\varnothing$ can be defined as $\varnothing = \varepsilon D m_s/E_{ph}$, where ε is the fraction of absorbed photons (here ε is 100% for 1 mm Ba_2AgIO_6), D is the dose rate, m_s is the mass of Ba_2AgIO_6 wafer, and E_{ph} is the X-ray energy.

Table S2 X-ray sensitivity of Ba_2AgIO_6 wafers at different thicknesses at 5 V/mm

thickness/mm	0.5	1.0	2.0
X-ray sensitivity /($\mu C \cdot Gy_{air} \cdot s^{-1} \cdot cm^{-2}$)	17.6	18.9	18.1

References

1. Yaffe M J, Rowlands J A. X-ray detectors for digital radiography. Physics in Medicine and Biology, 1997, 42(1): 1–39
2. Sakdinawat A, Attwood D. Nanoscale X-ray imaging. Nature Photonics, 2010, 4(12): 840–848
3. Tan Z, Pang J, Niu G, Yuan J H, Xue K H, Miao X, Tao W, Zhu H, Li Z, Zhao H, Du X, Tang J. Tailoring the electron and hole dimensionality to achieve efficient and stable metal halide

perovskite scintillators. Nanophotonics, 2021, 10(8): 2249–2256
4. Heiss W, Brabec C. Perovskites target X-ray detection. Nature Photonics, 2016, 10(5): 288–289
5. Yakunin S, Sytnyk M, Kriegner D, Shrestha S, Richter M, Matt G J, Azimi H, Brabec C J, Stangl J, Kovalenko M V, Heiss W. Detection of X-ray photons by solution-processed lead halide perovskites. Nature Photonics, 2015, 9(7): 444–449
6. Wei W, Zhang Y, Xu Q, Wei H, Fang Y, Wang Q, Deng Y, Li T, Gruverman A, Cao L, Huang J. Monolithic integration of hybrid perovskite single crystals with heterogenous substrate for highly sensitive X-ray imaging. Nature Photonics, 2017, 11(5): 315–321
7. Shrestha S, Fischer R, Matt G J, Feldner P, Michel T, Osvet A, Levchuk I, Merle B, Golkar S, Chen H, Tedde S F, Schmidt O, Hock R, Rührig M, Göken M, Heiss W, Anton G, Brabec C J. High-performance direct conversion X-ray detectors based on sintered hybrid lead triiodide perovskite wafers. Nature Photonics, 2017, 11(7): 436–440
8. Liu Y, Zhang Y, Zhu X, Feng J, Spanopoulos I, Ke W, He Y, Ren X, Yang Z, Xiao F, Zhao K, Kanatzidis M, Liu S F. Triple-cation and mixed-halide perovskite single crystal for high-performance X-ray imaging. Advanced Materials, 2021, 33(8): e2006010
9. European Union. Directive 2011/65/EU of the European Parliament and of the Council on the Restriction of the Use of Certain Hazardous Substances in Electrical and Electronic Equipment. 2002
10. Luo J, Li S, Wu H, Zhou Y, Li Y, Liu J, Li J, Li K, Yi F, Niu G, Tang J. $Cs_2AgInCl_6$ double perovskite single crystals: parity forbidden transitions and their application for sensitive and fast UV photodetectors. ACS Photonics, 2018, 5(2): 398–405
11. Li J, Tan Z, Hu M, Chen C, Luo J, Li S, Gao L, Xiao Z, Niu G, Tang J. Antimony doped Cs_2SnCl_6 with bright and stable emission. Frontiers of Optoelectronics, 2019, 12(4): 352–364
12. Luo J, Wang X, Li S, Liu J, Guo Y, Niu G, Yao L, Fu Y, Gao L, Dong Q, Zhao C, Leng M, Ma F, Liang W, Wang L, Jin S, Han J, Zhang L, Etheridge J, Wang J, Yan Y, Sargent E H, Tang J. Efficient and stable emission of warm-white light from lead-free halide double perovskites. Nature, 2018, 563(7732): 541–545
13. Pan W, Wu H, Luo J, Deng Z, Ge C, Chen C, Jiang X, Yin W, Niu G, Zhu L, Yin L, Zhou Y, Xie Q, Ke X, Sui M, Tang J. $Cs_2AgBiBr_6$ single-crystal X-ray detectors with a low detection limit. Nature Photonics, 2017, 11(11): 726–732
14. Volonakis G, Sakai N, Snaith H J, Giustino F. Oxide analogs of halide perovskites and the new semiconductor Ba_2AgIO_6. Journal of Physical Chemistry Letters, 2019, 10(8): 1722–1728
15. Yuan Y, Huang J. Ion migration in organometal trihalide perovskite and its impact on photovoltaic efficiency and stability. Accounts of Chemical Research, 2016, 49(2): 286–293
16. Shao Y, Fang Y, Li T, Wang Q, Dong Q, Deng Y, Yuan Y, Wei H, Wang M, Gruverman A, Shield J, Huang J. Grain boundary dominated ion migration in polycrystalline organic-inorganic halide perovskite films. Energy & Environmental Science, 2016, 9(5): 1752–1759
17. Sultana A, Wronski M M, Karim K S, Rowlands J A. Digital X-ray imaging using avalanche α-Se photoconductor. IEEE Sensors Journal, 2010, 10(2): 347–352
18. Berger M J, Hubbell J H, Seltzer S M, Chang J, Coursey J S, Sukumar R, Zucker D S, Olsen K. XCOM: Photon Cross Sections Database: NIST Standard Reference Database 8 (NIST, 2013)
19. Wei H, Fang Y, Mulligan P, Chuirazzi W, Fang H H, Wang C, Ecker B R, Gao Y, Loi M A, Cao L, Huang J. Sensitive X-ray detectors made of methylammonium lead tribromide perovskite single crystals. Nature Photonics, 2016, 10(5): 333–339
20. Toney J E, Schlesinger T E, James R B. Optimal bandgap variants of $Cd_{1-x}Zn_xTe$ for high-resolution X-ray and gamma-ray spectroscopy. Nuclear Instruments & Methods in Physics Research. Section A, Accelerators, Spectrometers, Detectors and Associated Equipment, 1999, 428(1): 14–24
21. Zheng W, Pang W, Meng G. Hydrothermal synthesis and characterization of perovskite-type Ba_2SbMO_6 (M = In, Y, Nd) oxides. Materials Letters, 1998, 37(4–5): 276–280
22. Tie S, Zhao W, Xin D, Zhang M, Long J, Chen Q, Zheng X, Zhu J, Zhang W H. Robust fabrication of hybrid lead-free perovskite pellets for stable X-ray detectors with low detection limit. Advanced Materials, 2020, 32(31): e2001981
23. Kim Y C, Kim K H, Son D Y, Jeong D N, Seo J Y, Choi Y S, Han I T, Lee S Y, Park N G. Printable organometallic perovskite enables large-area, low-dose X-ray imaging. Nature, 2017, 550(7674): 87–91
24. Martin J E. Radiation Detection and Measurement. New York: Wiley, 1989
25. Devanathan R, Corrales L R, Gao F, Weber W J. Signal variance in gamma-ray detectors—a review. Nuclear Instruments & Methods in Physics Research. Section A, Accelerators, Spectrometers, Detectors and Associated Equipment, 2006, 565(2): 637–649
26. Fraboni B, Ciavatti A, Merlo F, Pasquini L, Cavallini A, Quaranta A, Bonfiglio A, Fraleoni-Morgera A. Organic semiconducting single crystals as next generation of low-cost, room-temperature electrical X-ray detectors. Advanced Materials, 2012, 24(17): 2289–2293
27. Pan W, Yang B, Niu G, Xue K H, Du X, Yin L, Zhang M, Wu H, Miao X S, Tang J. Hot-pressed $CsPbBr_3$ quasi-monocrystalline film for sensitive direct X-ray detection. Advanced Materials, 2019, 31(44): e1904405
28. Xia M, Yuan J, Niu G, Du X, Yin L, Pan W, Luo J, Li Z, Zhao H, Xue K, Miao X, Tang J. Unveiling the structural descriptor of $A_3B_2X_9$ perovskite derivatives toward X-Ray detectors with low detection limit and high stability. Advanced Functional Materials, 2020, 30(24): 1910648
29. Konstantatos G, Badioli M, Gaudreau L, Osmond J, Bernechea M, de Arquer F P G, Gatti F, Koppens F H L. Hybrid graphene-quantum dot phototransistors with ultrahigh gain. Nature Nanotechnology, 2012, 7(6): 363–368

Longbo Yang received his Bachelor's degree in Electronic Science and Technology from Huazhong University of Science and Technology, China in 2019, and he is currently studying for a Master's degree in Optical Engineering at Wuhan National Laboratory for Optoelectronics, Huazhong University of Science and Technology. He is engaged in research on high-energy radiation detectors and halide perovskites for light emitting.

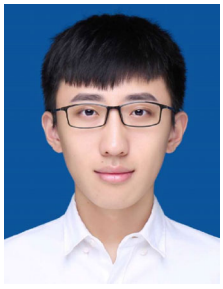

Jincong Pang received his Bachelor's degree in Optical Engineering from Huazhong University of Science and Technology, China in 2019, and he is currently studying for a Ph.D. degree in Optical Engineering at Wuhan National Laboratory for Optoelectronics, Huazhong University of Science and Technology. He is engaged in research on high-energy radiation detectors.

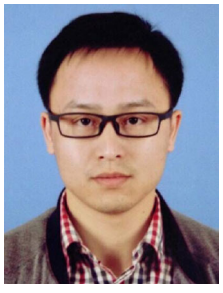

Zhifang Tan received his Master's degree from Huazhong Normal University, China in 2010, and Ph.D. degree in Applied Chemistry from Hiroshima University, Japan in 2014. Now he works toward Postdoctor in Wuhan National Laboratory for Optoelectronics, Huazhong University of Science and Technology, China. His research interest includes research and exploration of photoelectric materials, lead or lead-free perovskite materials.

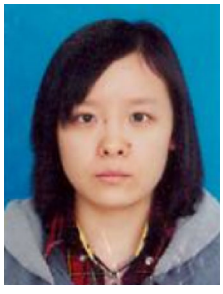

Qi Xiao received her Bachelor's degree and Ph.D. degree from Huazhong University of Science and Technology, China. She is now a postdoctoral researcher at Wuhan National Laboratory for Optoelectronics, Huazhong University of Science and Technology under the supervision of Prof. Jiang Tang. Her current research focuses on light emitting diodes.

Tong Jin received his Bachelor's degree in Optical Engineering from Huazhong University of Science and Technology, China in 2019, and he is currently studying for a master's degree in Optical Engineering at Wuhan National Laboratory for Optoelectronics, Huazhong University of Science and Technology. He is engaged in research on high-energy radiation detectors.

Jiajun Luo received his Bachelor's degree in 2015, and Ph.D. degree in Optical Engineering in 2020 both from Huazhong University of Science and Technology, China. He spent one year as a postdoctoral researcher at Wuhan National Laboratory for Optoelectronics, Huazhong University of Science and Technology in 2021. His research focuses on halide perovskites for light emitting and single crystals for X-ray detection.

Guangda Niu received his Bachelor's degree from School of Chemistry and Chemical Engineering, Nanjing University, China in 2011 and his Ph.D. degree from Department of Chemistry, Tsinghua University, China in 2016. In 2017, he joined Wuhan National Laboratory for Optoelectronics at Huazhong University of Science and Technology, China as an associate researcher. He is engaged in research on halogen perovskite and high-energy radiation detectors.

Jiang Tang received his Bachelor's degree from University of Science and Technology, China in 2003, and Ph.D. degree in Material Science and Engineering from University of Toronto, Canada in 2010. He spent one year and half as a postdoctoral researcher at IBM T. J. Watson Research Center and then joined in Wuhan National Laboratory for Optoelectronics, Huazhong University of Science and Technology, China as a professor in 2012. His group focuses on antimony selenide (Sb_2Se_3) thin film solar cells, halide perovskites nanocrystals for light emitting and single crystals for X-ray detection. He has published 150+ papers including *Nature*, *NatureMaterials*, *Nature Energy*, and *Nature Photonics*.